Robustness kriging-based optimization

Mélina Ribaud, Christophette Blanchet-Scalliet, Frederic Gillot, Céline Helbert

Robust optimization: a kriging-based multi-objective optimization approach

Mélina Ribaud[1,2], Christophette Blanchet-Scalliet[1], Frédéric Gillot[2,3], and Céline Helbert*[1]

[1]Univ Lyon, École centrale de Lyon, CNRS UMR 5208, Institut Camille Jordan, 36 avenue Guy de Collongue, F-69134 Ecully Cedex, France
[2]Univ Lyon, Ecole Centrale de Lyon, LTDS, CNRS UMR 5513, 36 avenue Guy de Collongue, F-69134 Ecully Cedex, France
[3]INRIA Rennes, I4S Team

January 30, 2019

Abstract

In the robust shape optimization's context, the evaluation cost of numerical models is reduced by the use of a response surface. Multi-objective methodologies for robust optimization that consist in simultaneously minimizing the function and a robustness criterion (the second moment) have already been developed. However, the efficient estimation of the robustness criterion in the framework of time-consuming simulation has not been much explored. A robust optimization procedure based on the prediction of the function and its derivatives by kriging is proposed. The second moment is replaced by an approximated version using Taylor expansion. A Pareto front is generated by a genetic algorithm named NSGA-II with a reasonable time of calculation.
Seven relevant strategies are detailed and compared with the same budget in two test functions (2D and 6D). In each case, we compare the results when the derivatives are observed and not. The procedure is also applied to an industrial case study where the objective is to optimize the shape of a motor fan.

Keywords. Robust Optimization, Gaussian process modelling, Multi-objective optimization, Taylor expansion, Expected Improvement.

1 Introduction

Complex physical phenomena are more and more studied through numerical simulations. These numerical models are able to mimic real experiments with a high accuracy. They predict the physical measures of interest (outputs) very precisely, but suffer form a heavy calculation cost. One main use of these simulations is to answer to optimization problem. This work focuses on cases where the optimized solution

*celine.helbert@ec-lyon.fr

is sensitive to inputs perturbations. For example, these perturbations are due to random fluctuations during production. A robust solution is then looked for. To solve the robust optimization problem, one way is to introduce a multi-objective optimization formulation where the first objective is the function itself and the second is a robustness criterion. These two objectives are often antagonistic. The issue of robust optimization is then to find a Pareto front that makes a balance between the optimization of the function and the impact of input perturbations (uncertainties). As the simulations given by the numerical code are often time-consuming, only a few simulations are then affordable. So, the computer code cannot be intensively exploited to provide the robust optimum. In this case, the optimization procedure is often run on a kriging model (see e.g [1]) that statistically approximates the computer code (kriging-based black-box optimization). Choosing where to sample the output in the input space to reach the optimum as fast as possible is a big issue. The authors in [2] developed the Efficient Global Optimization (EGO) algorithm that exploits the Expected Improvement (EI) criterion. However, the EGO algorithm is not an answer to the robust optimization problem because uncertainties are not taken into account.

In literature, a sample of works that handle robust optimization can be found. Methodologies depend of the kind of uncertainties. The authors in [3] propose two classes of uncertainties : uncertainties that "are primitively linked to the environment and condition of use" and uncertainties that "are those connected with the production/manufacturing process". In the first type of uncertainties, the aim is to find $\mathbf{x}$ such that $f(\mathbf{x}, \mathbf{U})$ is minimal with $\mathbf{U}$ a random vector (cf [4], [5], [6] and [7]). The authors in [4] propose to minimize the expectation of $f(\mathbf{x}, \mathbf{U})$ with a Gaussian process based methodology. The authors in [5] propose an algorithm that minimizes the worst-case. In all these sequential methods, the variables are clearly separated in two classes (design and uncertain) and the robust criterion is summed up either by the expectation or the worst-case.

In our context, manufacturing uncertainties are considered. The aim is to optimize the function $f(\mathbf{x}+\mathbf{H})$ where $\mathbf{x}$ are the design variables and $\mathbf{H}$ the perturbations. In [7] a mono-objective solution based on the worst-case on the response surface is proposed. In our work, we introduce a multi-objective strategy to detect the whole set of robust solutions. The first objective is the function itself (not the mean nor the worst-case) while the second objective is a robustness criterion which needs to be described.

The quantification of the robustness is challenging. [8], [9] and [10] give some overviews of different robustness criteria. Our industrial partners quantify the variability of a solution by the local variance of the output in a neighborhood of the solution (see e.g. [6] and [11]). Nevertheless the local variance is difficult to catch. A simpler formulation based on Taylor expansion as proposed by [12] is proposed. In the context of time consuming simulations, the criterion is predicted by kriging. Kriging is well adapted, since it can exploit the covariance structure between the GP model of the function and all the derivatives. This structure is described in [13] and used again by [14].

Then, the function and its robustness criterion are accessible through kriging. A multi-objective optimization is performed to provide solutions. In litterarure, several approaches (see [15] for an overview) mixing a GP modelling and multi-objective optimization are proposed: the aggregation methods (see [16], [17] and [18]), the Hypervolume methods (see [19], [20] and [21]), the maximin method (see [22]), the uncertainty reduction method (see [23])). [24] shows that the aggregation methods are not efficient

with a complex Pareto front. The hypervolume, maximin and uncertainty reduction algorithms need to make the multi-objective optimization on Gaussian processes. As the developed robustness criterion is not anymore Gaussian, it could be costly to adapt these methods in our case. Some optimization procedures inspired by [25] are proposed. These procedures consist in applying an evolutionary algorithm on the kriging predictions and taking into account kriging variance as suggested by [26].

The article is structured as follows. Our robustness kriging-based criterion is introduced in section 2. In section 3, the context of a Gaussian process metamodelling is introduced. The general multi-objective optimization scheme is presented in section 4 and the different enrichment strategies in section 5. The quality criteria to compare Pareto fronts are given in section 6. Finally, in section 7, the behavior of our methodology is studied on two toy functions and on an industrial test case.

2 Robustness criterion

The aim of this article is to conduct a robust optimization of a two times differentiable function

$$\begin{array}{rccc} f: & D \subset \mathbb{R}^p & \longrightarrow & [a;b] \subset \mathbb{R} \\ & \mathbf{x} & \longmapsto & f(\mathbf{x}) \end{array} \tag{1}$$

where p is the number of input variables, i.e. $x = (x_1, \ldots, x_p)$.

In this work, the robustness of f around a design point is assumed to be a local variance. More precisely, if $\mathbf{x} \in D$ is an observation point, the variability of function f around $\mathbf{x}$ is supposed to be catched by $v_f(\mathbf{x}) = Var\left(f(\mathbf{x}+\mathbf{H})\right)$ where $\mathbf{H}$ represents fluctuations that can appear during fabrication. The production error $\mathbf{H}$ follows a centred Gaussian distribution. Then $\mathbf{H} \sim \mathcal{N}(0_{\mathbb{R}^d}, \Delta^2)$ where Δ^2 is defined by:

$$\Delta^2 = \begin{pmatrix} \delta_1^2 & 0 & \ldots & 0 \\ 0 & \delta_2^2 & \ddots & 0 \\ \vdots & \ddots & \ddots & \vdots \\ 0 & \ldots & 0 & \delta_p^2 \end{pmatrix}$$

Variances $\delta_1, \ldots, \delta_p$ associated to each input are not necessary the same and are given by experts.

A point $\mathbf{x}^1 \in D$ is considered less robust than a point $\mathbf{x}^2 \in D$ if $v_f(\mathbf{x}^1) > v_f(\mathbf{x}^2)$. In Figure 1, the minimum on the right (circles) is less robust than the one on the left (triangles). Let $\mathbf{h}^1, \ldots, \mathbf{h}^N$, $\mathbf{h}^j \in \mathbb{R}^p$, $j = 1, \ldots, N$ be N realizations of $\mathbf{H}$. The empirical estimation of the variance $v_f(\mathbf{x})$ is:

$$\widehat{v}_f(\mathbf{x}) = \frac{1}{N-1} \sum_{j=1}^{N} \left(f(\mathbf{x}+\mathbf{h}^j) - \bar{f}(\mathbf{x})\right)^2 \tag{2}$$

where $\bar{f}(\mathbf{x}) = \frac{1}{N}\sum_{j=1}^{N}\left(f(\mathbf{x}+\mathbf{h}^j)\right)$ is the empirical mean (first moment). The estimation of the variance around only one point needs N calls to f.
To obtain an estimation of $v_f(\mathbf{x})$ with an error lower than $\epsilon > 0$ with a probability $1-\alpha$, N should

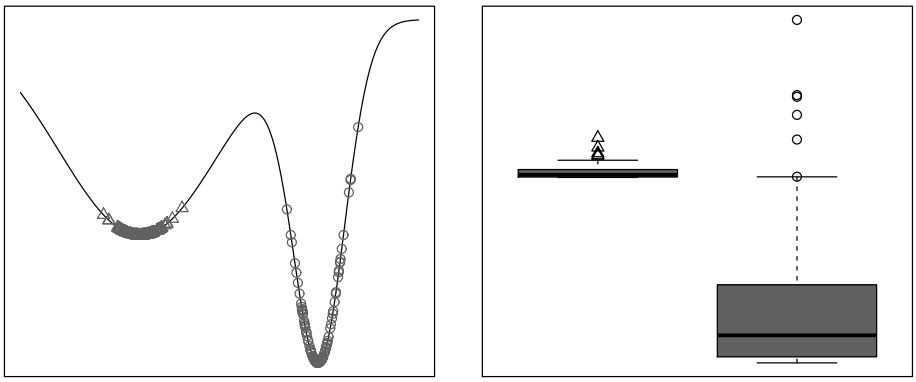

Figure 1: Illustration of the robustness. The figure on the left shows a function in one dimension with two optima, the right one (circles) is the less robust. The figure on the right shows the variability of the points simulated by the same Gaussian law around the two optima.

satisfy the following inequality :

$$N \geq \left(z_{1-\alpha/2}^2 \frac{\hat{\mu}_4 - \left(s_f^2\right)^2}{\epsilon^2} \right) \tag{3}$$

where s_f^2 and $\hat{\mu}_4$ are estimations of the second and the fourth central moment, $z_{1-\alpha/2}$ is the quantile of risk $\alpha/2$ of the standard normal distribution. In practice N is too high to allow the empirical assessment of the variance on f. To overcome this problem, the robustness is quantified using a Taylor approximation, as proposed for example in [12].

For all $\mathbf{h} \in \mathbb{R}^p$, one has:

$$f(\mathbf{x}+\mathbf{h}) = f(\mathbf{x}) + \nabla_f(\mathbf{x}) \cdot \mathbf{h} + \frac{1}{2}\mathbf{h}'\mathbb{H}_f(\mathbf{x})\mathbf{h} + o(\|\mathbf{h}\|^2)$$

where ∇_f is the gradient of f and $\mathbb{H}_f$ the Hessian matrix of f. Let

$$\widetilde{f}(\mathbf{x}+\mathbf{h}) = f(\mathbf{x}) + \nabla_f(\mathbf{x}) \cdot \mathbf{h} + \frac{1}{2}\mathbf{h}'\mathbb{H}_f(\mathbf{x})\mathbf{h}$$

Then, the robustness criterion is defined by the following approximation of the local variance :

$$RC_f(\mathbf{x}) = Var\left(\widetilde{f}(\mathbf{x}+\mathbf{H})\right)$$

An analytical form of this expression is given by the following expression (see [27]):

$$RC_f(\mathbf{x}) = tr\left(\nabla_f(\mathbf{x})\nabla_f(\mathbf{x})'\Delta^2\right) + \frac{1}{2}tr\left(\mathbb{H}_f^2(\mathbf{x})(\delta_1^2,\ldots,\delta_p^2)(\delta_1^2,\ldots,\delta_p^2)'\right) \tag{4}$$

where tr is the matrix trace. If the output of a simulation provides the results of the function and the first derivatives, RC_f criterion can be computed with only one call to the computer code. However in the context of costly simulations, a robust optimization cannot be directly done on f and RC_f.
The next section presents how with a kriging approach these quantities can be predicted.

3 Gaussian process modelling for the function and its derivatives

As it can be seen in Equation (4), the robustness criterion depends on the first and second derivatives of f. A Gaussian process metamodel (see [14]) is well suited to this context in the sense that all derivatives can easily be predicted. In this section, the model, the predictions are presented and illustrated on a toy example.

3.1 Kriging Model

Let a function f supposed as a realization of a Gaussian process $(Y(\mathbf{x}))_{\mathbf{x}\in D}$ with a constant mean, μ, and with a stationary covariance function $k(\mathbf{x},\tilde{\mathbf{x}}) = \sigma^2 r_{\boldsymbol{\theta}}(\mathbf{x}-\tilde{\mathbf{x}})$, $\forall(\mathbf{x},\tilde{\mathbf{x}}) \in D\times D$. This process is assumed to be two-times differentiable in mean square at point $(\mathbf{x},\tilde{\mathbf{x}})$.
We denote by $(Y_{x_i}(\mathbf{x}))_{\mathbf{x}\in D} = \left(\frac{\partial Y}{\partial x_i}(\mathbf{x})\right)_{\mathbf{x}\in D}$ the first-order partial derivative of $(Y(\mathbf{x}))_{\mathbf{x}\in D}$ with respect to x_i and by $\left(Y_{x_i,x_j}(\mathbf{x})\right)_{\mathbf{x}\in D} = \left(\frac{\partial^2 Y}{\partial x_i \partial x_j}(\mathbf{x})\right)_{\mathbf{x}\in D}$ the second-order partial derivative of $(Y(\mathbf{x}))_{\mathbf{x}\in D}$ with respect to x_i and x_j.

All the covariance structures between the process and its derivatives are then well known and are given by :

$$cov\left(Y(\mathbf{x}), \frac{\partial Y(\tilde{\mathbf{x}})}{\partial \tilde{x}_j}\right) = \frac{\partial k(\mathbf{x},\tilde{\mathbf{x}})}{\partial \tilde{x}_j},$$
$$cov\left(\frac{\partial Y(\mathbf{x})}{\partial x_i}, \frac{\partial Y(\tilde{\mathbf{x}})}{\partial \tilde{x}_j}\right) = \frac{\partial^2 k(\mathbf{x},\tilde{\mathbf{x}})}{\partial x_i \partial \tilde{x}_j}/$$

Let $(x^1,\dots,x^n)$ be the initial design of experiments, where $x^k \in D, 1 \le k \le n$. The evaluation of the function (resp. first and second derivatives) at point $\mathbf{x}^k$ is denoted by $y^k \in \mathbb{R}$ (resp. $y^k_{x_i} \in \mathbb{R}$ and $y^k_{x_i,x_j} \in \mathbb{R}$), where $i \in \{1,\dots,p\}$, $j \in \{i,\dots,p\}$ and $k \in \{1,\dots,n\}$. The collection of outputs $\mathbf{y}$, $\mathbf{y}_{x_i}$ and $\mathbf{y}_{x_i,x_j}$ is such that :

$$\mathbf{y} = (y^1,\dots,y^n)'$$
$$\mathbf{y}_{x_i} = (y^1_{x_i},\dots,y^n_{x_i})'$$
$$\mathbf{y}_{x_i,x_j} = (y^1_{x_i,x_j},\dots,y^n_{x_i,x_j})'$$

$(y^k, y^k_{x_1},\dots,y^k_{x_p}, y^k_{x_1,x_1},\dots,y^k_{x_i,x_j},\dots,y^k_{x_p,x_p})$, $k \in \{1,\dots,n\}$ is then a realization of the following $d = 1 + \frac{3p}{2} + \frac{p^2}{2}$ dimensional GP:

$$Z(\mathbf{x}) = (Y(\mathbf{x}), Y_{x_1}(\mathbf{x}),\dots,Y_{x_p}(\mathbf{x}), Y_{x_1,x_1}(\mathbf{x}),\dots,Y_{x_i,x_j}(\mathbf{x}),\dots,Y_{x_p,x_p}(\mathbf{x}))',\ 1 \le i \le p,\ i \le j \le p$$

at points $\mathbf{x}^1,\dots,\mathbf{x}^n$.

3.2 Kriging predictions

The problem is to predict Z considering observations at points $\mathbf{x}^1,\dots,\mathbf{x}^n$. But, the entire vector Z is not always observable. Let $u_{obs} \subset \{1,\dots,d\}$ be the components that are observable. For example,

only the function and its first derivatives can be affordable. In the same way it is not always necessary to predict the whole vector Z. Let $u_{pred} \subset \{1, \dots, d\}$ be the components that need to be predicted. In the following we suppose that $1 \in u_{obs}$ and we denote $f_{obs} = (1, 0_{\mathbb{R}^{d_{obs}-1}}, \dots, 1, 0_{\mathbb{R}^{d_{obs}-1}})' \in \mathbb{R}^{nd_{obs}}$, $d_{obs} = \#u_{obs}$ and $f_{pred} = (1, 0_{\mathbb{R}^{d_{pred}-1}})' \in \mathbb{R}^{d_{pred}}$, $d_{pred} = \#u_{pred}$. The kriging mean is then given by the following equation :

$$\widehat{\mathbf{z}}_{u_{pred}}(\mathbf{x}) = \widehat{\mu} f_{pred} + \mathbf{c}_{\boldsymbol{\theta}}(\mathbf{x})' \boldsymbol{\Sigma}_{\boldsymbol{\theta}}^{-1} (\mathbf{z}_{u_{obs}} - \widehat{\mu} f_{obs}), \quad \widehat{\mathbf{z}}_{u_{pred}}(\mathbf{x}) \in \mathbb{R}^{d_{pred}} \tag{5}$$

where $\mathbf{z}_{u_{obs}} = \begin{pmatrix} z_{obs}^1 \\ \vdots \\ z_{obs}^n \end{pmatrix}$ the observation vector. $\widehat{\mathbf{z}}_{u_{pred}}(\mathbf{x})$ is the prediction vector and

$$\widehat{\mu} = (f_{obs}' \Sigma_\theta^{-1} f_{obs})^{-1} f_{obs}' \Sigma_\theta^{-1} \mathbf{z}_{u_{obs}}.$$

The mean square error (MSE) at point $\mathbf{x} \in D$ is given by :

$$\widehat{\mathbf{s}}_{u_{pred}}^2(\mathbf{x}) = \boldsymbol{\Sigma}_{\boldsymbol{\theta}}(\mathbf{x}, \mathbf{x}) - \begin{pmatrix} f_{pred} & \boldsymbol{c}_{\boldsymbol{\theta}}(\mathbf{x}) \end{pmatrix} \begin{pmatrix} 0 & f_{obs}' \\ f_{obs} & \boldsymbol{\Sigma}_{\boldsymbol{\theta}} \end{pmatrix}^{-1} \begin{pmatrix} f_{pred}' \\ \boldsymbol{c}_{\boldsymbol{\theta}}(\mathbf{x}) \end{pmatrix}, \quad \widehat{\mathbf{s}}_{u_{pred}}^2(\mathbf{x}) \in \mathcal{M}_{d_{pred} \times d_{pred}}$$

where $\boldsymbol{\Sigma}_{\boldsymbol{\theta}}$ is the covariance matrix of size $nd_{obs} \times nd_{obs}$ given by :

$$\boldsymbol{\Sigma}_{\boldsymbol{\theta}} = \begin{pmatrix} \Sigma_{\mathbf{x}_1, \mathbf{x}_1}(u_{obs}, u_{obs}) & \dots & \Sigma_{\mathbf{x}_1, \mathbf{x}_n}(u_{obs}, u_{obs}) \\ \vdots & \ddots & \vdots \\ \Sigma_{\mathbf{x}_n, \mathbf{x}_1}(u_{obs}, u_{obs}) & \dots & \Sigma_{\mathbf{x}_n, \mathbf{x}_n}(u_{obs}, u_{obs}) \end{pmatrix}$$

and

$$\Sigma_{\mathbf{x}, \tilde{\mathbf{x}}} = \begin{pmatrix} \Sigma_{Y,Y} & \Sigma_{Y,Y_{\tilde{x}_j}} & \Sigma_{Y,Y_{\tilde{x}_j \tilde{x}_k}} & \Sigma_{Y,Y_{\tilde{x}_j^2}} \\ \Sigma_{Y_{x_i},Y} & \Sigma_{Y_{x_i},Y_{\tilde{x}_j}} & \Sigma_{Y_{x_i},Y_{\tilde{x}_j \tilde{x}_k}} & \Sigma_{Y_{x_i},Y_{\tilde{x}_j^2}} \\ \Sigma_{Y_{x_i x_l},Y} & \Sigma_{Y_{x_i x_l},Y_{\tilde{x}_j}} & \Sigma_{Y_{x_i x_l},Y_{\tilde{x}_j \tilde{x}_k}} & \Sigma_{Y_{x_i x_l},Y_{\tilde{x}_j^2}} \\ \Sigma_{Y_{x_i^2},Y} & \Sigma_{Y_{x_i^2},Y_{\tilde{x}_j}} & \Sigma_{Y_{x_i^2},Y_{\tilde{x}_j \tilde{x}_k}} & \Sigma_{Y_{x_i^2},Y_{\tilde{x}_j^2}} \end{pmatrix}$$

$i, j, k, l \in \{1, \dots p\}$ with $l > i$ and $k > j$. For instance $\Sigma_{Y_{x_i},Y_{\tilde{x}_j}} = cov(Y_{x_i}, Y_{\tilde{x}_j}) = cov(\eta_{x_i}, \eta_{\tilde{x}_j}) = \frac{\partial^2 k(\mathbf{x} - \tilde{\mathbf{x}})}{\partial x_i \partial \tilde{x}_j}$. The matrix $\mathbf{c}_{\boldsymbol{\theta}}(\mathbf{x}) \in \mathcal{M}_{nd_{obs} \times d_{pred}}$ is the covariance matrix between $Z_{u_{pred}}(\mathbf{x})$ and the observations and the matrix $\boldsymbol{\Sigma}_{\boldsymbol{\theta}}(\mathbf{x}, \mathbf{x}) \in \mathcal{M}_{d_{pred} \times d_{pred}}$ is the variance of $Z_{u_{pred}}(\mathbf{x})$.

3.3 Illustration with the six-hump Camel function

In this section different kriging-based response surfaces conditioning or not on derivatives are compared. The chosen toy function is the six-Hump Camel function defined by:

$$f(\mathbf{x}) = \left(4 - 2.1x_1^2 + \frac{x_1^4}{3}\right) x_1^2 + x_1 x_2 + \left(-4 + 4x_2^2\right) x_2^2, \mathbf{x} \in [-2; 2] \times [-1; 1]$$

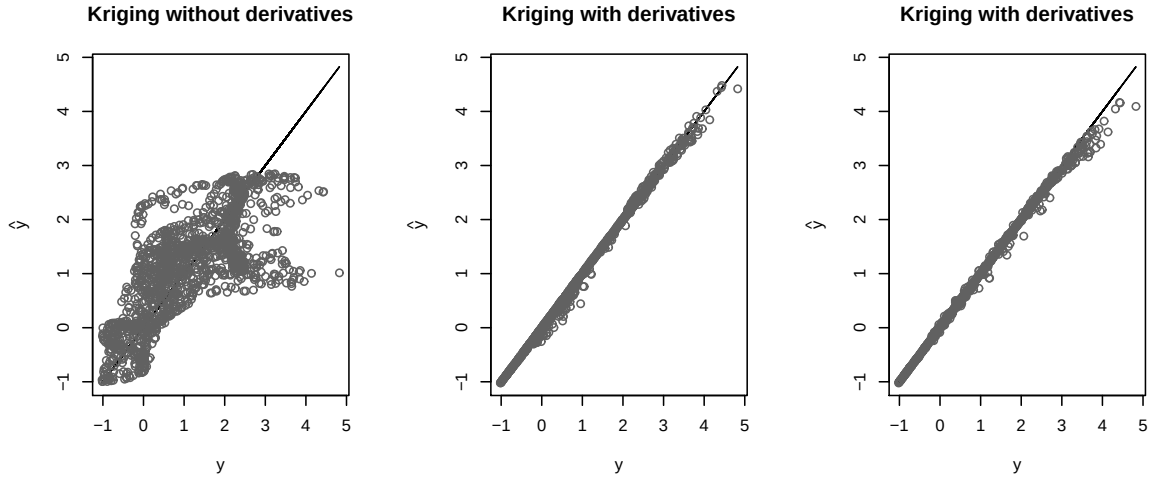

Figure 2: Prediction plots for the six-hump Camel function: 10 points without observation of the derivatives (on the left), 10 points with 5 derivatives (on the middle) and 60 points without observation of the derivatives (on the right).

The kriging covariance kernel is a tensor product one:

$$cov\left(Y(\mathbf{x}), Y(\tilde{\mathbf{x}})\right) = k(\mathbf{x} - \tilde{\mathbf{x}}) = \sigma^2 \prod_{j=1}^{p} \rho_{\theta_j}\left(|x_j - x'_j|\right), \ \boldsymbol{\theta} = (\theta_1, \ldots, \theta_p) \in \mathbb{R}_+^p \tag{6}$$

where ρ_{θ_j} is a correlation function which only depends on the one dimensional range parameter θ_j, see e.g [1] and [28]. A Matern 5/2 kernel is used because the output is supposed to be two times continuously differentiable:

$$\forall \theta \in \mathbb{R}^+, \forall h \in \mathbb{R}^+, \rho_\theta(h) = \left(1 + \frac{\sqrt{5}|h|}{\theta} + \frac{5h^2}{3\theta^2}\right) \exp\left(-\frac{\sqrt{5}|h|}{\theta}\right).$$

The kriging predictive quality has been compared in different learning situations :

- 10 learning points where f is observed (left part of Figure 2)
- 10 learning points where f and all the derivatives are observed (middle part of Figure 2)
- 60 learning points where f is observed (right part of Figure 2)

The learning sets composed of 10 or 60 points are maximin latin hypercube samplings. The test set is a latin hypercube sampling of 1500 points. As expected, the left and middle parts of Figure 2 show that kriging with derivatives performs much better than without. If computing one derivative costs as much as computing a new point, it can be observed on the right part of Figure 2 that kriging without derivatives does better. But in industrial applications, computing derivatives is often more affordable.

4 Robust optimization procedure

In this section, the robust optimization procedure that uses our criterion (see Equation (8)) is presented. The robust optimization problem is written as:

Find the Pareto set $\mathbb{X}_0$, solution of the following multi-objective optimization

$$\min_{\mathbf{x}\in\mathbb{R}^p}\{f(\mathbf{x}), RC_f(\mathbf{x})\} \tag{7}$$

The approach to solve it in the context of time consuming simulations is based on a classical black-box optimization scheme (see [2]). The optimization scheme (see Figure 3) is based on the following steps :

- **Initialization.** The costly function and possibly its derivatives are evaluated on a well chosen initial design of experiments. A kriging model is adjusted on this first set of outputs. Two response surfaces $\{\hat{obj}_f(x)\}$ and $\{\hat{obj}_{RC_f}(x)\}$ related to the two objectives $\{f(x)\}$ and $\{RC_f(x)\}$ are predicted.
  Remarks : in the different case studies, the chosen initial design is a Maximin Latin Hypercube Sampling (Maximin HLS) (see [29]).

- **Loop until the budget is reached**

  1. **Multi-objective optimization.** A multi-objective global optimization method is applied to solve $\min_{\mathbf{x}\in\mathbb{R}^p}\{\hat{obj}_f(x), \hat{obj}_{RC_f}(x)\}$. A Pareto front is identified.
     Remarks : NSGA II algorithm is chosen for its good performances to find complex Pareto fronts.
  2. **Enrichment.** A set of q points is selected from the Pareto front. The function and possibly its derivatives are evaluated on these new points. The Gaussian process model and the two response surfaces are updated.

The aim of this section is to define the two response surfaces to be optimized. Next section focuses on different stategies to select good points from the Pareto front.

Three different response surfaces have been studied to run the multi-objective methodology. The first approach consists in optimizing the predicted version of the function and the robustness criterion. This approach, quite crude, is denoted by the "plug in" approach in the following and is described below. The second one is based on the famous Expected Improvement quantity in order to take into account prediction uncertainty. The third one is the most complex : it optimizes the multipoint Expected Improvement versions of $\{f(x)\}$ and $\{RC_f(x)\}$.

4.1 The "plug in" response surfaces

Recall that $\widehat{z}(\mathbf{x})$ from Equation (5) is

$$\widehat{z}(\mathbf{x}) = \left(\widehat{y}(\mathbf{x}), \ldots, \widehat{y}_{x_p,x_p}(\mathbf{x})\right)'$$

The prediction of the true function f is given by the first coordinate of the vector $\widehat{z}(\mathbf{x})$.
The prediction of $RC_f(\mathbf{x})$ is defined by:

$$RC_{\widehat{y}}(\mathbf{x}) = tr\left(\nabla_{\widehat{y}}(\mathbf{x})\nabla_{\widehat{y}}(\mathbf{x})'\Delta^2\right) + \frac{1}{2}tr\left(\mathbb{H}^2_{\widehat{y}}(\mathbf{x})(\delta_1^2, \ldots, \delta_p^2)'(\delta_1^2, \ldots, \delta_p^2)\right) \tag{8}$$

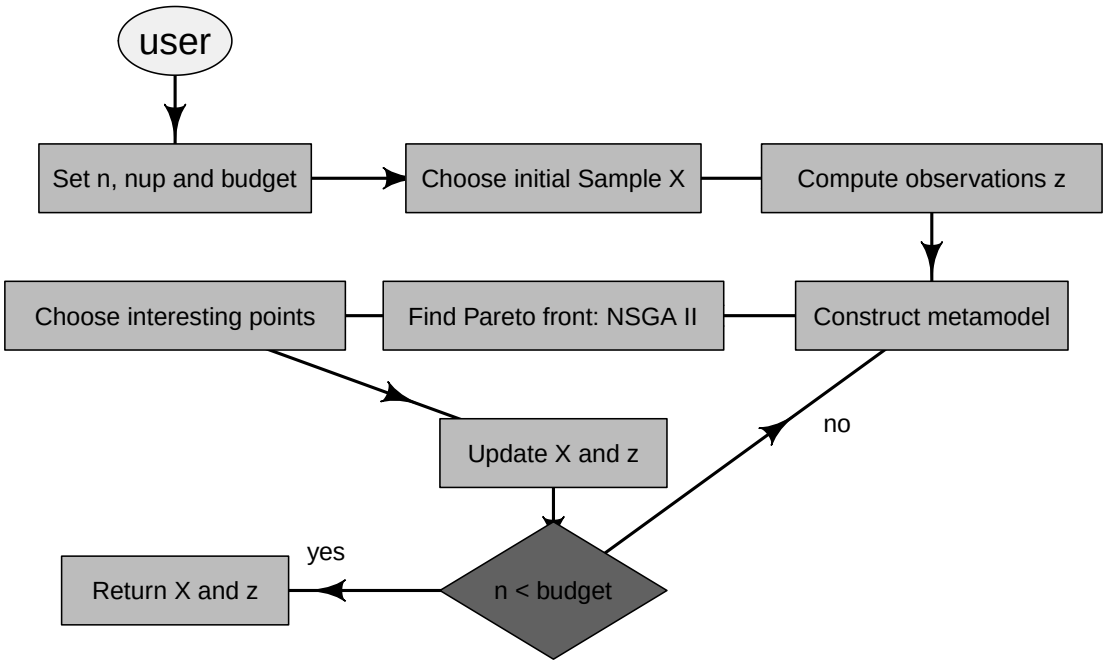

Figure 3: The robust optimization procedure.

where $\nabla_{\widehat{y}}$ is the vector $\begin{pmatrix} \widehat{y}_{x_1} \\ \vdots \\ \widehat{y}_{x_p} \end{pmatrix}$ and is the prediction of the gradient. $\mathbb{H}_{\widehat{y}}$ is the matrix $\begin{pmatrix} \widehat{y}_{x_1,x_1} & \cdots & \widehat{y}_{x_1,x_p} \\ \vdots & \ddots & \vdots \\ \widehat{y}_{x_p,x_1} & \cdots & \widehat{y}_{x_p,x_p} \end{pmatrix}$ and corresponds to the prediction of the Hessian matrix. $\nabla_{\widehat{y}}$ and $\mathbb{H}_{\widehat{y}}$ are obtained from different components of $\widehat{z}(x)$.

The **"plug in" formulation** is then :

Find the Pareto set $\mathbb{X}_0$, solution of the following multi-objective optimization

$$\min_{\mathbf{x}\in\mathbb{R}^p} \{\widehat{y}(\mathbf{x}), RC_{\widehat{y}}(\mathbf{x})\} \tag{9}$$

Remarks :

- The definition of the predicted robustness criterion corresponds to the definition of Equation (4) where the derivatives have been replaced by their prediction.
- These response surfaces are easy to compute. NSGA II on these quantities is run faslty. But prediction uncertainty is not taken into account at this stage.

4.2 The "Expected improvement" response surfaces

Unlike the previous case, in this approach we take into account the kriging variance in the optimization scheme. The best way to do it is to optimize the expected improvement.

In the EGO algorithm, the expected improvement (EI) criterion measures the improvement of a point $\mathbf{x}$ in the minimization of function f and is used to add new points to the learning set. The expression of the EI (cf [2]) at point $\mathbf{x}$ is:

$$EI(\mathbf{x}) = \mathbb{E}\left[(\min(y(\mathbb{X})) - Y(\mathbf{x}))^+ \,|Y(\mathbb{X}) = \mathbf{y}\right]$$

where $\min(y(\mathbb{X})) = \min(y^1, \ldots, y^n)$.
The analytical expression of the EI for a Gaussian process is given by:

$$EI(\mathbf{x}) = (\min(y(\mathbb{X}) - \widehat{y}(\mathbf{x}))\Phi\left(\frac{\min(y(\mathbb{X})) - \widehat{y}(\mathbf{x})}{\widehat{s}(\mathbf{x})}\right) + \widehat{s}(\mathbf{x})\phi\left(\frac{\min(y(\mathbb{X})) - \widehat{y}(\mathbf{x})}{\widehat{s}(\mathbf{x})}\right)$$

where $\widehat{y}(\mathbf{x})$ is the kriging mean, $\widehat{s}(\mathbf{x})$ is the kriging standard deviation, Φ and ϕ are the cdf and pdf of the standard normal law.

In our case, these formulas have to be adapted :

i) to the robustness criterion,

ii) to a larger set of observations that can possibly include derivatives,

iii) to a multi-objective optimization context.

To answer to i) we need to define the process $(RC_Y(\mathbf{x}))_{\mathbf{x}\in D}$. From Equation 4 the process is naturally defined by:

$$RC_Y(\mathbf{x}) = tr\left(\nabla_Y(\mathbf{x})\nabla_Y(\mathbf{x})'\Delta^2\right) + \frac{1}{2}tr\left(\mathbb{H}_Y^2(\mathbf{x})(\delta_1^2, \ldots, \delta_p^2)'(\delta_1^2, \ldots, \delta_p^2)\right) \tag{10}$$

where ∇_Y is the vector $\begin{pmatrix} Y_{x_1} \\ \vdots \\ Y_{x_p} \end{pmatrix}$ and $\mathbb{H}_Y$ is the matrix $\begin{pmatrix} Y_{x_1,x_1} & \ldots & Y_{x_1,x_p} \\ \vdots & \ddots & \vdots \\ Y_{x_p,x_1} & \ldots & Y_{x_p,x_p} \end{pmatrix}$.

To answer to point ii) , conditional expectation are considered over observations of vector z that includes derivatives when they are available.

Eventually to answer to iii) the authors in [25] show that, in the context of multi-objective optimization, the usual reference value which is the current observed minimum is too constraining. To still allowing improvement, this reference value is rather taken as the worst value on the current Pareto front. The expressions of the EI for f and RC_f are then the following:

$$EI_y(\mathbf{x}) = \mathbb{E}\left[(\max(y(\mathbb{X}^*)) - Y(\mathbf{x}))^+ \,|Z(\mathbb{X}) = \mathbf{z}_{u_{obs}}\right]$$
$$EI_{RC_y}(\mathbf{x}) = \mathbb{E}\left[(\max(RC_y(\mathbb{X}^*)) - RC_Y(\mathbf{x}))^+ \,|Z(\mathbb{X}) = \mathbf{z}_{u_{obs}}\right]$$

where $\mathbb{X}^*$ is the set of non-dominated points for the objectives $\{y, RC_y\}$ of the learning set $\mathbb{X}$.

The **"Expected improvement" formulation** is then :

Find the Pareto set $\mathbb{X}_0$, solution of the following multi-objective optimization

$$\min_{\mathbf{x}\in\mathbb{R}^p}\{EI_y(\mathbf{x}), EI_{RC_y}(\mathbf{x})\} \tag{11}$$

Remarks:

- A solution $\mathbf{x}^1$ dominates another solution $\mathbf{x}^2$ for the m objectives $g_1, \ldots, g_m$ if and only if $\forall i \in \{1, \ldots, m\}$ $g_i(\mathbf{x}^1) \leq g_i(\mathbf{x}^2)$ and $\exists i \in \{1, \ldots, m\}$ $g_i(\mathbf{x}^1) < g_i(\mathbf{x}^2)$. Among a set of solution $\mathbb{X}$, the non-dominated set $\mathbb{X}^*$ (Pareto front) are those that are not dominated by any member of the set $\mathbb{X}$.
- When the derivatives used to compute the robustness criterion are not observed we replace them by the kriging prediction in $\max(RC_y(\mathbb{X}^*))$.
- The link between $RC_Y(\mathbf{x})$ and $Z(\mathbf{x})$ being not linear, the process $(RC_Y(\mathbf{x}))_{\mathbf{x}\in D}$ is not Gaussian anymore. EI_{RC_y} is then estimated by a Monte Carlo method.

4.3 The "Multipoint Expected improvement" response surfaces

The EI makes a good balance between exploration and minimization but it computes the improvement of a single point. The multi-point EI (q-EI) is used to measure the improvement of q points $\mathbf{X} = (\mathbf{x}^{n+1}, \ldots, \mathbf{x}^{n+q})'$ ([30]). In a multi-objective context the expressions of the q-EI are:

$$qEI_y(\mathbf{X}) = \mathbb{E}\left[\left(\max(y(\mathbb{X}^*)) - \min(Y(\mathbf{x}^{n+1}), \ldots, Y(\mathbf{x}^{n+q}))\right)^+ |\mathbf{z}_{u_{obs}}\right]$$
$$qEI_{RC_y}(\mathbf{X}) = \mathbb{E}\left[\left(\max(RC_y(\mathbb{X}^*)) - \min(RC_Y(\mathbf{x}^{n+1}), \ldots, RC_Y(\mathbf{x}^{n+q}))\right)^+ |\mathbf{z}_{u_{obs}}\right]$$

The **"Multipoint Expected improvement" formulation** is then :

Find the Pareto set $\mathbb{X}_0$, solution of the following multi-objective optimization

$$\min_{\mathbf{X}\in\mathbb{R}^{p\times q}}\{-qEI_y(\mathbf{X}), -qEI_{RC_y}(\mathbf{X})\}$$

5 Sequential stategy for the enrichment

Seven enrichment strategies based on the three approaches described above have been developed. Once the Pareto front is found (NGSAII algorithm), points are chosen to enrich the set of observations. Different strategies can be studied. They are described below.

5.1 Enrichment for the "plug in" formulation

With this approach, it is not costly to find the Pareto front since the response surfaces are easily computed. But the kriging variance has never been considered. If kriging predictions turn out to be of poor quality, some interesting areas can be missed. Hence the first stategy consists in choosing part of the points from the Pareto front but also part of the points randomly in the parameter space. Other stategies consist in using information from the kriging variance, for example through an expected improvement criterion.

More precisely five enrichment approaches have been benchmarked and are described below:

1. MyAlea: $\lfloor \frac{q}{2} \rfloor$ [1] points are selected randomly on the Pareto front and $q - \lfloor \frac{q}{2} \rfloor$ points are randomly chosen in the parameter space.

2. MyEI: $-EI_y$ as well as $-EI_{RC_y}$ are computed for each point of the Pareto front. A k-means clustering using the method of [31] is applied to the non-dominated points of $\{-EI_y, -EI_{RC_y}\}$ to provide q clusters. Then the q clusters' medoids are added to the design.

3. MyqEI: a simulated annealing algorithm gives the set of q points among the Pareto front that minimizes the function $-qEI_y - qEI_{RC_y}$.

Two sequential approaches presented in [30] can be used as the replacement of the q-EI to measure the improvement of q points: the Kriging Believer and the Constant Liar.

4. MyKB: q points are sequentially selected from the Pareto front based on the Kriging Beliver strategy. The $-EI_y$ and $-EI_{RC_y}$ are computed on the Pareto front, then a point $\mathbf{x}_0^1$ is randomly chosen from the EI Pareto front and added. $\widehat{y}(\mathbf{x}_0^1)$ is then considered known and is assumed to be equal to $\widehat{y}(\mathbf{x}_0^1)$. Another computation of $-EI_y$ and $-EI_{RC_y}$ provides one more point based on the same strategy up to the q requested points.

5. MyCL: q points are sequentially selected based on the Constant Liar strategy. The $-EI_y$ and $-EI_{RC_y}$ are computed on the Pareto front, then a point $\mathbf{x}_0^1$ is randomly chosen from the EI Pareto front and added. $y(\mathbf{x}_0^1)$ is then considered known and is assumed to be equal to $\min y(\mathbb{X}^*)$. Another computation of $-EI_y$ and $-EI_{RC_y}$ provides one more point based on the same strategy up to the q requested points.

The problem with this group of strategies is that kriging variance is not taken into account during the multi-objective optimization. Except for the MyAlea strategy, some interesting areas can be missed. The second approach solves this issue by conducting the multi-objective optimization directly on the EI.

5.2 Enrichment for the "expected improvement" formulation

The multi-objective optimization is performed on the EI of the output and the robustness criterion. This approach takes into account the kriging variance from the beginning of the procedure. For this approach, one enrichment strategy is proposed to add one point by one point:

6. MEIyAlea: a point is randomly chosen and sequentially added until the total budget is reached.

Because this strategy adds points sequentially one by one ($q = 1$) the last formulation is introduced to add points by batch.

5.3 Enrichment for the "multi-point expected improvement" formulation

One last enrichment approach is proposed to add q points simultaneously :

7. MqEIyAlea: one point is randomly extracted from the Pareto front, this point will provide q points in the parameter space for the next optimization step.

The seven methods to perform the enrichment are summarized in Table 1.

[1] $\lfloor . \rfloor$ is the floor function

Method	Minimization	Interesting points	Updates
MyAlea	y, RC_y	Random points on the Pareto front and the parameters space	Batch
MyEIClust	y, RC_y	Cluster on EIy and EIRCy	Batch
MyqEI	y, RC_y	Annealing algorithm on qEIy and qEIRCy	Batch
MyKB	y, RC_y	Kriging believer	Batch
MyCL	y, RC_y	Constant liar	Batch
MEIyAlea	EI_y, EI_{RC_y}	Random point on the Pareto front	Seq
MqEIyAlea	qEI_y, qEI_{RC_y}	Random point on the Pareto front	Batch

Table 1: Minimization problems and methods to choose the interesting points.

6 Quality criteria for Pareto fronts

The seven strategies based on three different response surfaces are compared through the quality of the found Pareto front. Several measures exist to quantify the quality of a Pareto front (cf [32], [33], [34] and [35]). The Inverted Generational Distance (IGD) and the Hypervolume (HV) are selected here to compare strategies. Let $\mathbf{f} = (f_1, \ldots, f_m)$ be the objective functions, $\mathcal{P}$ the theoretical Pareto front and $\mathbb{X}^*$ the empirical Pareto front where $M = \#\mathcal{P}$. The chosen performance metrics are:

- Inverted Generational Distance (IGD) see [36]:

$$IGD(\mathbb{X}^*) = \sqrt{\frac{1}{M}\sum_{i=1}^{M} d_i^2}$$

  where $d_i = \min_{\mathbf{x}\in\mathbf{X}^*}(\|\mathbf{f}(\mathbf{x}^i) - \mathbf{f}(\mathbf{x})\|_2)$, $\mathbf{f}(\mathbf{x}^i) \in \mathcal{P}$. This metric evaluates the distance between the empirical and the theoretical Pareto front. A small value is better.

- Hypervolume (HV) see [35]. Figure 4 shows the Hypervolume (HV) of a Pareto front. [37] introduce an algorithm to compute this volume. The empirical HV is compared to the theoretical one. The Hypervolume depends of the reference point. When it is possible the nadir point of the true Pareto front is used. Then the Hypervolume enables the comparaison of two empirical fronts.

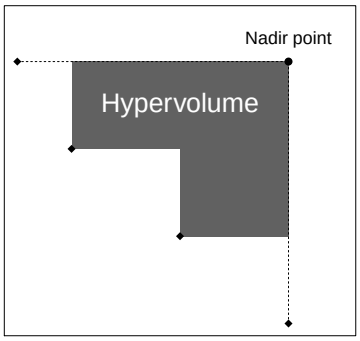

Figure 4: Diamonds represent the individuals of the empirical Pareto front $\mathbb{X}^*$. The black circle is the Nadir point of the set $\mathbb{X}^*$.

7 Applications

This section compares the strategies on two toy functions and one industrial test case. The toy function are the six-hump Camel in two dimensions and the Hartmann in six dimensions. Two cases are considered depending on whether the derivatives are affordable or not. For the sake of efficiency only three of the best strategies are applied on Hartmann function and on the industrial test case. Along applications NSGA II is performed with populations of a hundred points. Each generation is done with a crossed probability of 1 and a mutation probability of $\frac{1}{p}$, where p is the inputs' number.

7.1 Six-hump Camel function: 2D

In this application, the six-hump Camel function is considered. The two input variables are affected by uncertainties that are modeled with a Gaussian distribution with a standard deviation of $\delta_j = \frac{0.05}{4}(\max(x_j) - \min(x_j))$, $j = \{1, 2\}$. Then:

$$(\mathbf{x} + \mathbf{H}) \sim \mathcal{N}\left(\mathbf{x}, \begin{pmatrix} \delta_1^2 & 0 \\ 0 & \delta_2^2 \end{pmatrix}\right)$$

Figure 5 shows the four optimal areas for the robust optimization in the objectives and parameters space.

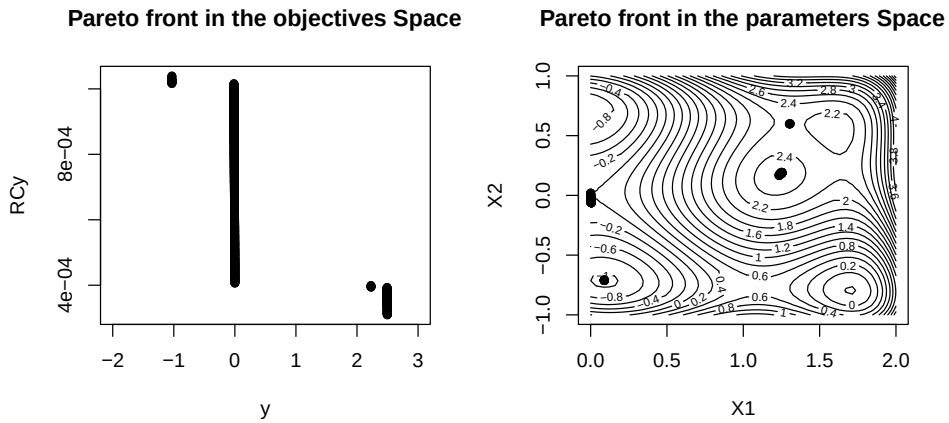

Figure 5: Pareto front of the six-hump Camel function in the objectives space (left) and in the parameters space (right).

In order to perform a robust optimization, the function and all the first and second derivatives need to be predicted. The set of predicted indexes is $u_{pred} = \{1, \ldots, 6\}$ and corresponds to the following vector:

$$Z_{u_{pred}} = (Y, Y_{x_1}, Y_{x_2}, Y_{x_1,x_2}, Y_{x_1,x_1}, Y_{x_2,x_2})$$

7.1.1 Derivatives' observations

In this first part of the study, the function and all derivatives are available at each evaluated point. The set of observed indexes is $u_{obs} = \{1, \ldots, 6\}$ that corresponds to the vector of processes:

$$Z_{u_{obs}} = (Y, Y_{x_1}, Y_{x_2}, Y_{x_1,x_2}, Y_{x_1,x_1}, Y_{x_2,x_2})$$

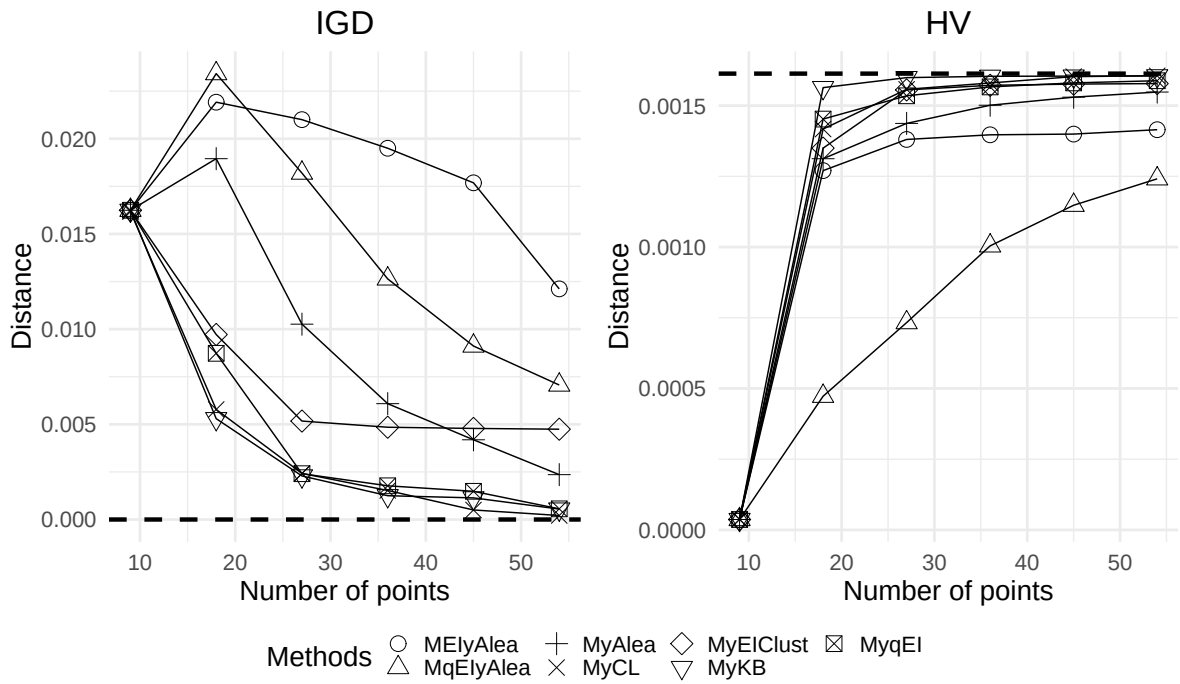

Figure 6: Six-hump Camel function with derivatives' observations. Evolution of the Pareto metrics with the number of points compute for all the methods over 100 different runs of the algorithm. The HV value of the theoretical front is represented by the dotted line.

The initial learning set is a maximin LHS of nine points. Nine updates of five points are added for a total budget of 54 points. The optimization scheme is performed 100 times with different initial learning sets to compare the seven strategies.

Method	Updates	Computation time	Nb areas
MyAlea	Batch	2 min	1.83
MyEIClust	Batch	2 min	2.73
MyqEI	Batch	6 min 30 sec	2.85
MyKB	Batch	3 min	3.77
MyCL	Batch	3 min	3.68
MEIyAlea	Seq	1 h	1.61
MqEIyAlea	Batch	3 h 30 min	3.06

Table 2: Summary of the results obtained with the seven strategies on 100 simulations on the six-hump Camel function with derivatives' observation. The true number of areas is 4.

Results are provided in Figure 6 and Table 2. In the table, two criteria are used to compare the methods: the computation time and the number of areas found after 54 evaluations. In the figure, the methods are compared through two Pareto front performance metrics.

Our analysis is as follow: the MyKB and MyCL are the two most efficient strategies in terms of metrics, found areas and computation time. Then MyqEI, MEIClust and MqEIyAlea give good results for the metrics and the areas. Even if MyqEI is quite better in metrics and MqEIyAlea in areas. Finally MyAlea and MEIyAlea are the worst efficient methods in areas and metrics. In addition, MEIyAlea and

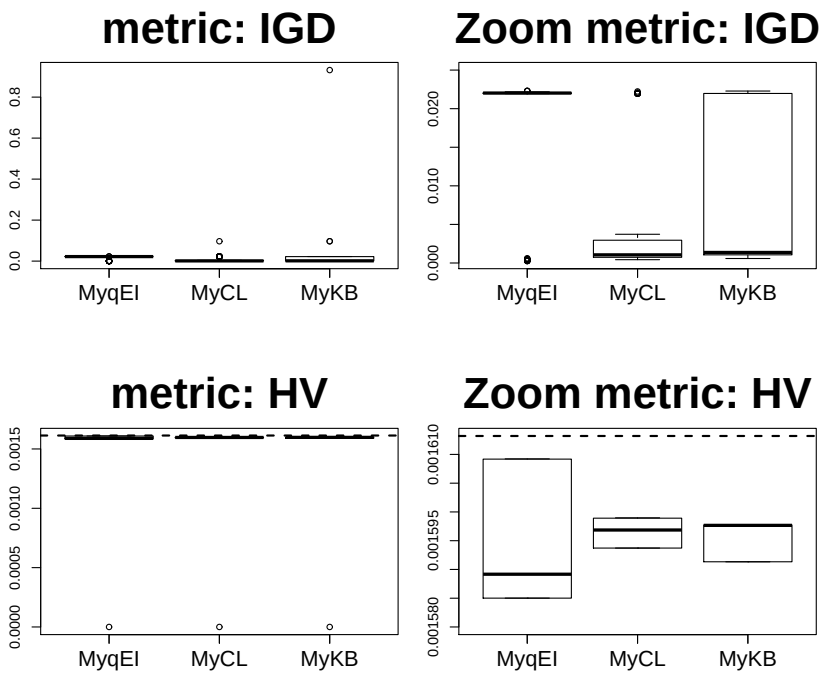

Figure 7: Boxplots of the metrics computed for the three best methods over 100 simulations for the six-hump Camel function with derivative observations.

MqEIyAlea are really time consuming. Then, the best methods selected to be used for robust optimization in limited budget applications are MyqEI, MyCL and MyKB, which fully exploit batch computation of EI without excessive computational cost. Figure 7 shows the boxplots of these three methods for each distance. MyqEI gives the worst results in mean. It comes from the annealing simulation of the strategy that is difficult to tune.

7.1.2 No derivatives' observations

The aim of this section is to analyze the behavior of the seven strategies when the derivatives' observations are not available.
The observed indexes set is $u_{obs} = \{1\}$ and the predicted indexes set is $u_{pred} = \{1, \dots, 6\}$ that corresponds to the processes vectors:

$$Z_{u_{obs}} = Y$$
$$Z_{u_{pred}} = (Y, Y_{x_1}, Y_{x_2}, Y_{x_1,x_2}, Y_{x_1,x_1}, Y_{x_2,x_2})$$

The initial sample set is still a maximin LHS of 9 points. The available information is poorer, the detection of the front need to add more points. That's why 35 updates of 5 points are performed until a total budget of 324 points. The optimization scheme is performed 100 times with different initial learning sets to compare the seven strategies.

Results are provided in Figure 8 and Table 3. Our analysis is as follow : the six hump Camel function is difficult to be approximated without derivatives' observations. MyAlea strategy which is partially based on a random search gives the best results. In this context, too much reliance should not be placed upon

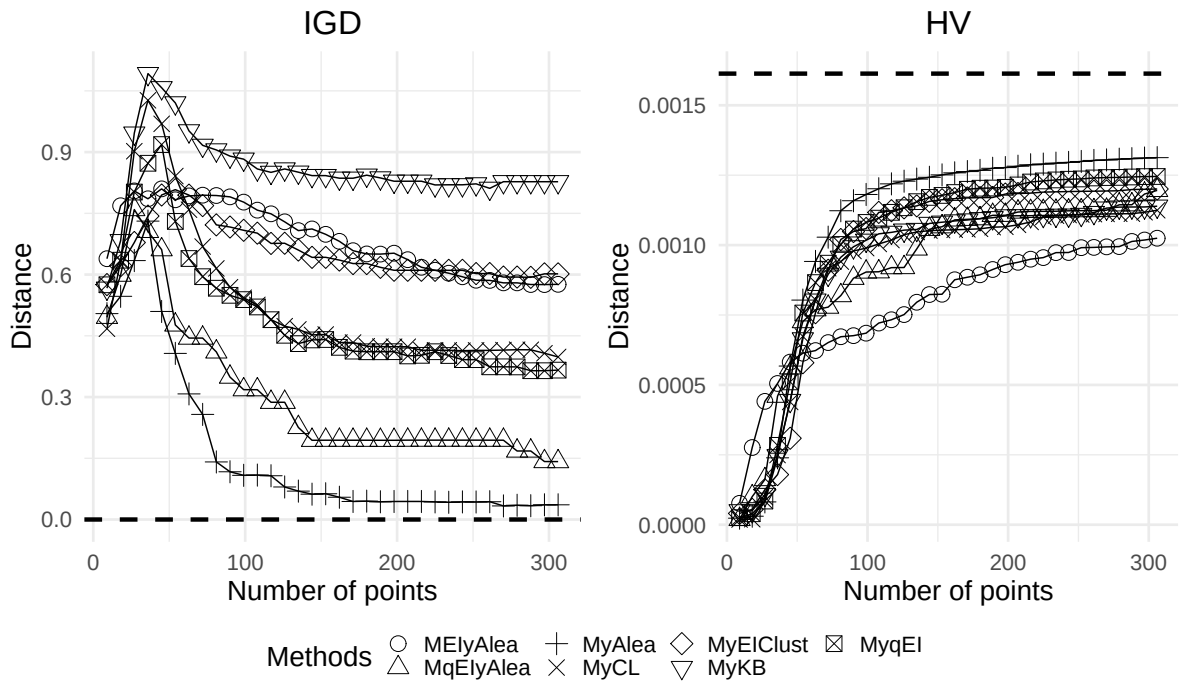

Figure 8: Six-hump Camel function without derivatives' observations. Evolution of the Pareto metrics with the number of points compute for all the methods over 100 different runs of the algorithm. The HV value of the theoretical front is represented by the dotted line.

Method	Updates	Computation time	Nb areas
MyAlea	Batch	18 min	2.98
MyEIClust	Batch	11 min	1.94
MyqEI	Batch	58 min	2.53
MyCL	Batch	15 min	2.58
MyKB	Batch	15 min	1.91
MEIyAlea	Seq	5 h 47 min	1.15
MqEIyAlea	Batch	15h17 min	3.57

Table 3: Summary of the results obtained with the seven strategies on 100 simulation on the six-hump Camel function without derivatives' observation. The true number of areas is 4.

kriging. MyqEI and MqEIyAlea provide quite good results because they use the qEI criterion. This takes into account the improvement provided by a batch of points of the front. However, MqEIyAlea is too time consuming. The MyCL strategy that does not trust the response surface gives quite good results too, contrary to the MyKB. Finally, the MyEIClust and MEIyAlea strategies that use the EI criterion provide poor results. Even, if the MyEIClust strategy is quite better thanks to the clustering used to enrich the set. The best strategy is MyAlea but MyqEI and MyCL are also retained in order to test them in higher dimension.

7.2 Hartmann function: 6D

In this section, the three best strategies identified in Section 7.1.1 are benchmarked in higher dimension (six). A Gaussian process model is built with a tensor product kernel with the Matern5_2 covariance

function (see Equation 6). The studied function is the six-dimensional Hartmann function defined by:

$$f(\mathbf{x}) = -\sum_{i=1}^{4} \alpha_i exp\left(-\sum_{j=1}^{6} A_{ij}(x_j - P_{ij})^2\right) x_1^2,\ \mathbf{x} \in [0;1]^2$$

with $\alpha = (1, 1.2, 3, 3.2)'$,

$$A = \begin{pmatrix} 10 & 3 & 17 & 3.5 & 1.7 & 18 \\ 0.05 & 10 & 17 & 0.1 & 8 & 14 \\ 3 & 3.5 & 1.7 & 10 & 17 & 8 \\ 17 & 8 & 0.05 & 10 & 0.1 & 14 \end{pmatrix}$$

and

$$P = 10^{-4} \begin{pmatrix} 1312 & 1696 & 5569 & 124 & 8283 & 5886 \\ 2329 & 4135 & 8307 & 3736 & 1004 & 9991 \\ 2348 & 1451 & 3522 & 2883 & 3047 & 6650 \\ 4047 & 8828 & 8732 & 5743 & 1091 & 381 \end{pmatrix}$$

The random variables are x_4 and x_5 and follow a centred Gaussian distribution with a standard deviation of $\delta_j = \frac{0.05}{4}(\max(x_j) - \min(x_j))$, $j = \{4, 5\}$.
Like previously, two cases are considered depending upon whether derivatives' observations are provided or not.

7.2.1 Derivatives' observations

The observed indexes set is $u_{obs} = u_{pred} = \{1, 5, 6, 20, 26, 27\}$ that corresponds to the vector of processes:

$$Z_{u_{obs}} = Z_{u_{pred}} = (Y, Y_{x_4}, Y_{x_5}, Y_{x_4,x_5}, Y_{x_4,x_4}, Y_{x_5,x_5})$$

The initial sample set is a maximin LHS composed of 18 points. Five updates are made and 18 points are added by update for a total budget of 108 points. The best methods found in the previous test case with derivatives informations: MyqEI, MyCL and MyKB strategies are applied.

The left part of Figure 9 shows that the three methods converge to the true front. At step 2, MyqEI gives the more advanced front. At the final step, the three methods perform very well (see the right part of Figure 9). MyKB and MyCL take 10 minutes for the five steps when MyqEI takes 12 minutes.

7.2.2 No derivatives' observations

The indexes set is $u_{obs} = \{1\}$ and $u_{pred} = \{1, 5, 6, 20, 26, 27\}$ that corresponds to the processes vector

$$\begin{aligned} Z_{u_{obs}} &= Y \\ Z_{u_{pred}} &= (Y, Y_{x_4}, Y_{x_5}, Y_{x_4,x_5}, Y_{x_4,x_4}, Y_{x_5,x_5}) \end{aligned}$$

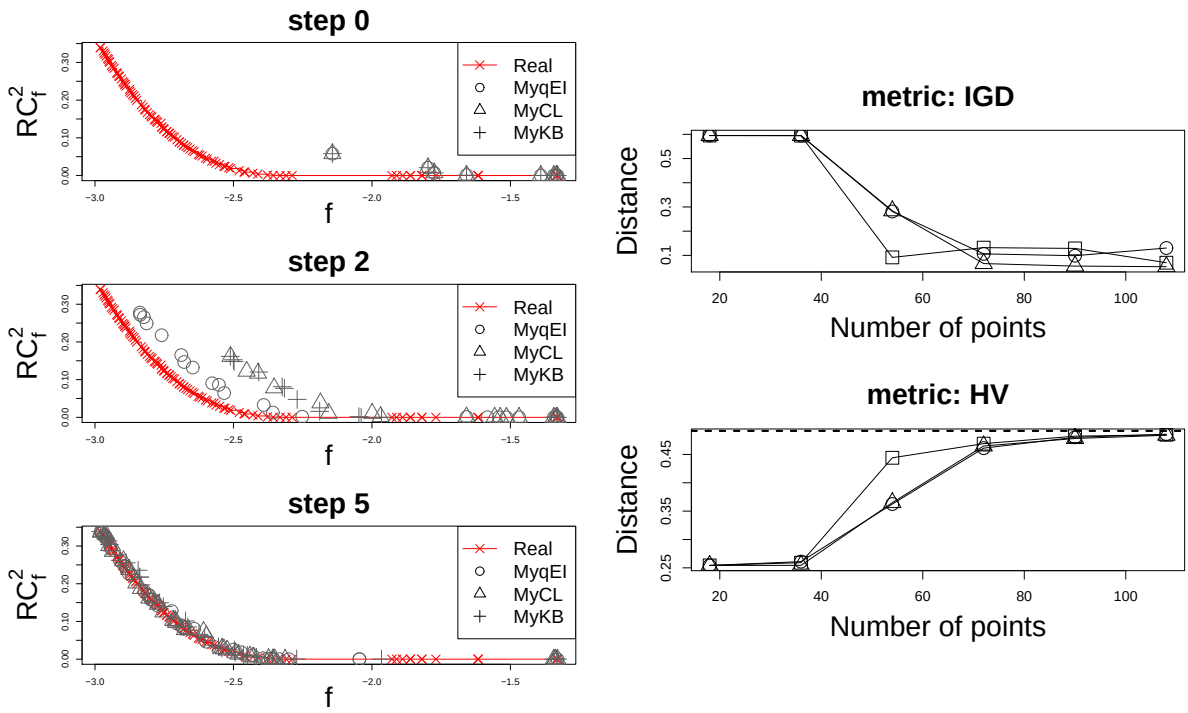

Figure 9: On the left: Pareto fronts obtained during the optimization procedure of the three strategies at initial step (step 0), middle step (step 2) and final step (step 5). On the right: evolution of the metrics computed during the algorithm for all the methods over 100 simulations for the Hartmann function with derivatives' observations. The HV value of the theoretical front is represented by the dotted line.

The initial design is still a maximin LHS composed of 18 points. More updates are provided since derivatives are not affordable. Here 35 updates of 18 points are sequentially computed until a total budget of 648 points. The best methods identified previously: MyAlea, MyqEI and MyCL strategies are applied.

The left part of Figure 10 shows that the three methods converge to the true front. At step 5, all methods have almost found the entire front. The bottom part of the front is difficult to localize even with 578 additional points. The right part of Figure 10 shows that the distance starts to converge to the expected value in the 100 first points. For the IGD metric, the values are subject to little perturbations around the expected value zero. For the HV measure, the three methods converge to the theoretical value with only 100 points that correspond to 6 updates. MyAlea takes 1h15min, MyqEI takes 1h40min and MyCL takes 1h04min for the 35 steps.

7.3 Industrial test case

The chosen application is an automotive fan. In a cooling system, the fan is used to maintain a constant flow of air through the radiator. The shape of fans has constantly evoluated with time. It results from a compromise between aerodynamics and acoustics performances. Over time, the geometry has become more and more complex to satisfy increasingly stringent requirements. Consequently, the number of parameters that describe the fan shape has really increased. Besides, due to complexity increase of the numerical modelling, simulations become very time consuming. At last, the efficiency of produced fans is reduced because of uncertainties that result in disturbances on the geometrical inputs. Therefore, a optimal use of the simulations are necessary to robustly optimized the design of a fan.

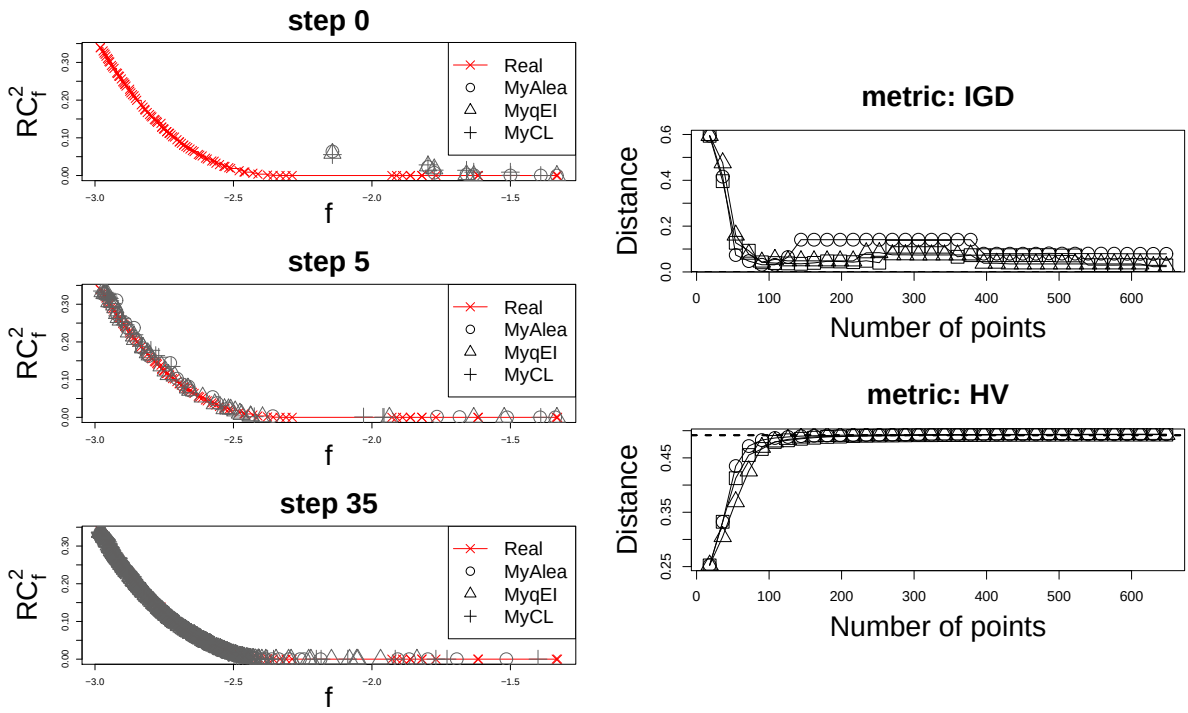

Figure 10: On the left: Pareto fronts obtained during the optimization procedure of the three strategies at initial step (step 0), step 5 and final step (step 35). On the right: evolution of the metrics during the algorithm compute for all the methods in 100 simulations for the Hartmann function with no derivatives' observation. The HV value of the theoretical front is represented by the dotted line.

Each fan blade is characterized by the chord length, the stagger and the maximal camber height (Hmax) at five sections. Figure 11 shows a blade section with the parametrization. In the following, the parameters are noted $\mathbf{x} = (x_1, \ldots, x_{15}) \in D$. Among these inputs, only the three middle stagger are uncertain (x_7, x_8, x_9). They follow a normal distribution such that $X_i \sim \mathcal{N}(x_i, \delta_i^2)$, $i = \{7, 8, 9\}$. The variances δ_i^2 are given by the industrial experts (see Table 4). The first and second derivatives of the uncertain variables are provided by the numerical code.

Input	Chord length					Stagger					Hmax				
Section	1	2	3	4	5	1	2	3	4	5	1	2	3	4	5
Notation	x_1	x_2	x_3	x_4	x_5	x_6	x_7	x_8	x_9	x_{10}	x_{11}	x_{12}	x_{13}	x_{14}	x_{15}
Min	0.04	0.06	0.08	0.09	0.11	-50.67	-59.68	-65.87	-70.29	-73.58	3.82	3.82	3.82	2.86	1.91
Max	0.07	0.09	0.11	0.14	0.16	-45.85	-54	-59.59	-63.6	-66.57	5.73	5.73	5.73	4.29	2.86
δ	0	0	0	0	0	0	1.16	1.28	1.36	0	0	0	0	0	0

Table 4: Inputs of the numerical code. Hmax is the maximal camber height. These inputs are considered at 5 different sections from section 1 to 5.

The initial sample set is a maximin LHS of 46 observations. Figure 12 shows the learning sample set in the true objectives space $\{\eta, RC_\eta\}$. η represents the real costly efficiency function and RC_η the robustness criterion calculated on η given by the Equation (4). The total budget is composed of 136 points, 90 points are added to the initial design along 5 updates of 18 points. The three best methods (MyCL, MyKB and MyqEI) used in Section 7.2.1 are selected to conduct the robust optimization.

Figure 13 shows that at the final step, MyCL, MyKB and MyqEI have added points in the same interesting

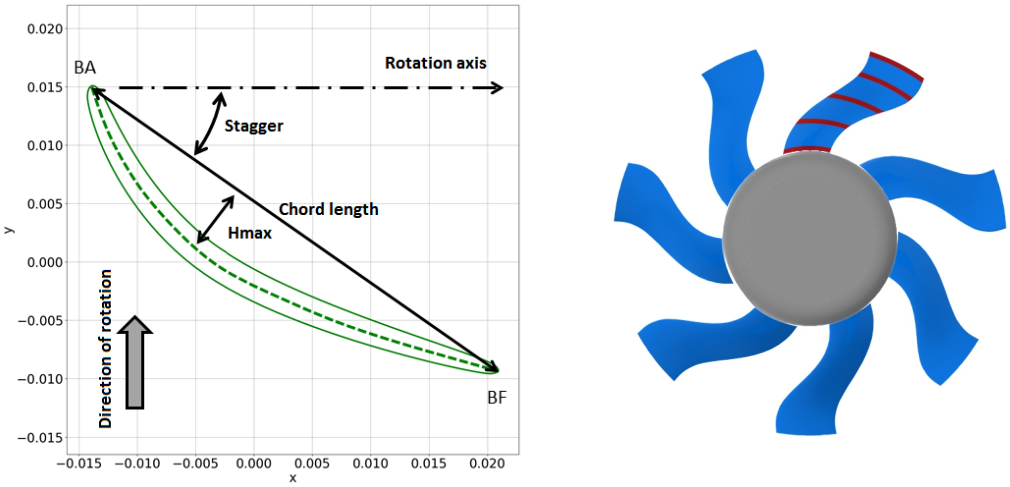

Figure 11: Blade section with the three input parameters on the left. Sections are represented on the right by the red lines along one blade. Section 1 are the closest to the disc and section 5 the most far away.

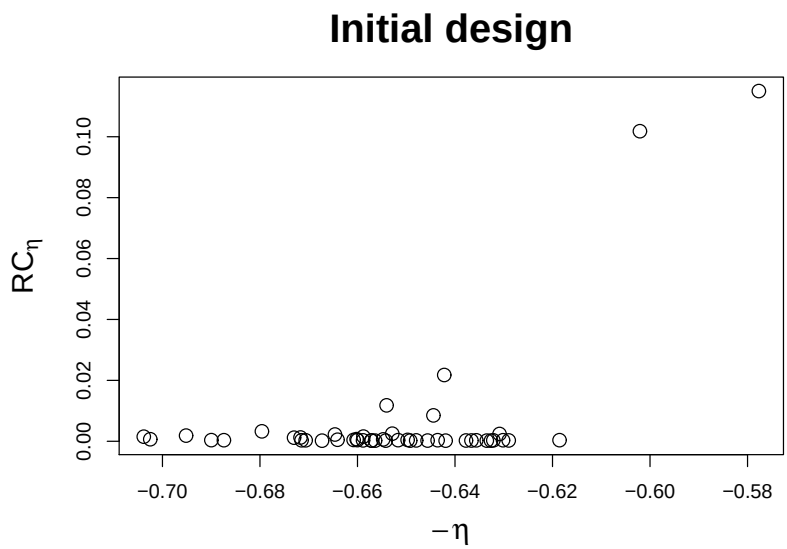

Figure 12: The 46 initial observation points in the true objectives space: opposite efficiency ($-\eta$) and robustness criterion calculated on the efficiency (RC_η).

	Update	1	2	3	4	5	Total
MyCL	Time	0h18	0h30	0h 40	1h00	1h00	3h28
MyKB	Time	0h18	0h31	0h 44	1h00	1h01	3h34
MyqEI	Time	0h16	0h25	0h 36	0h48	1h00	3h05

Table 5: Computation time for the three strategies MyCL, MyKB and MyqEI.

area. MyCL provides the worst progress in the objectives' space. MyqEI gives the most dispersed area and MyKB the most progressed ones. These differences come from the way where strategies add points along updates. As it can be seen on Figures 15 that the three methods progress in the same interesting area. However, the MyqEI adds points in two different areas at the first update (on the middle and at the

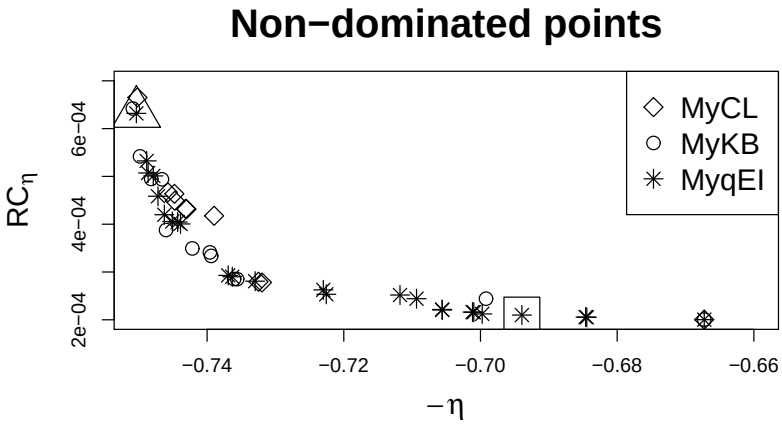

Figure 13: Non-dominated points of the final design for methods MyCL, MyKB and MyqEI in the true objectives space: opposite efficiency ($-\eta$) and robustness criterion calculated on the efficiency (RC_η).

bottom right), this explains why the MyqEI strategy gives the most dispersed front. MyCL and MyKB progress in the same way, MyCL more slowly however.

Table 5 shows that MyqEI is the fastest strategy. To conclude, the three strategies give the same interesting non-dominated points that are compromises between efficiency and robustness. The shape of two of these compromises (see big square and triangle on Figure 13) are represented on Figure 14.

Figure 14: The shape on the left corresponds to the square of Figure 13 and those on the right to the triangle.

8 Conclusion

In this article we propose an efficient kriging-based robust optimization procedure. The methodology rests on a multi-objective optimization of the function and a robustness criterion simultaneously. The robustness criterion is defined as a Taylor expansion of the local variance. This expression using derivatives has the benefit of being easily predicted under Gaussian process modelling. The introduced multi-objective strategies are iterative and based on two steps : a NSGA-II algorithm performed on predicted versions of the two objectives and a relevant enrichment composed of a batch of points well chosen from the Pareto front. Seven strategies have been compared on two toy functions. The study reveals that it is much more computerwise efficient to optimize the plug in versions of kriging prediction rather than EI. In that case when the points are selected using kriging variance, the procedure detects all the diversity of the robust solutions. Finally, the methodology is applied on an industrial problem that consists in optimizing the motor fan shape taking into account production uncertainties. Interesting shapes are provided to answer to the robust optimization of the turbomachinary efficiency, that are good compromise between efficiency and robustness.

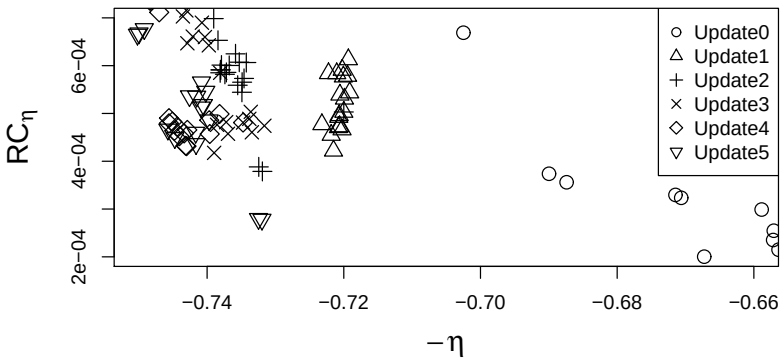

(a) Method MyCL

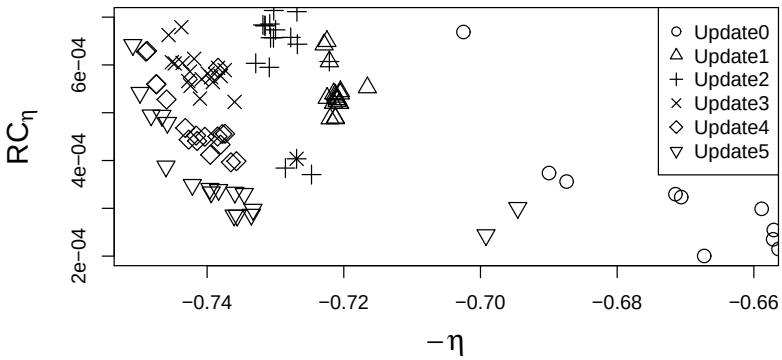

(b) Method MyKB

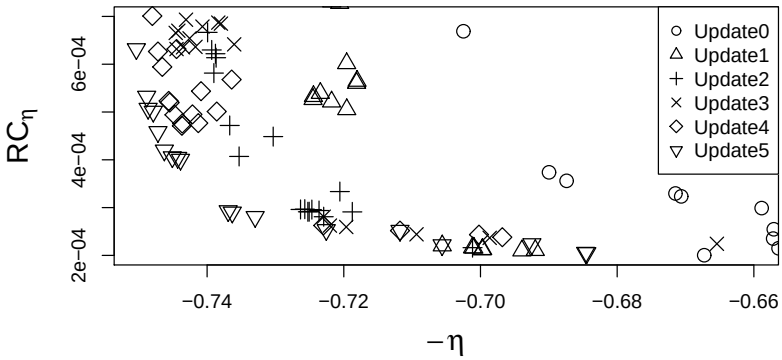

(c) Method MyqEI

Figure 15: Progression of the algorithm for the method MyCL (a), MyKB (b), MyqEI (c) in the true objectives space: opposite efficiency ($-\eta$) and robustness criterion calculated on the efficiency (RC_η).

Acknowledgments

This work benefited from the financial support of the French ANR project "PEPITO" (ANR-14-CE23-0011). We also thank the LMFA (Laboratory of Fluid, Mechanics and Acoustics form Ecole Centrale de Lyon) that provides the numerical codes of the industrial test case.

References

[1] Thomas J. Santner, Brian J. Williams, and William I. Notz. *The design and analysis of computer experiments*. Springer Series in Statistics. Springer-Verlag, New York, 2003.

[2] Donald R Jones, Matthias Schonlau, and William J Welch. Efficient global optimization of expensive black-box functions. *Journal of Global optimization*, 13(4):455–492, 1998.

[3] Nicolas Lelièvre, Pierre Beaurepaire, Cécile Mattrand, Nicolas Gayton, and Abdelkader Otsmane. On the consideration of uncertainty in design: optimization - reliability - robustness. *Structural and Multidisciplinary Optimization*, 54(6):1423–1437, Dec 2016.

[4] Janis Janusevskis and Rodolphe Le Riche. Simultaneous kriging-based estimation and optimization of mean response. *Journal of Global Optimization*, 55(2):313–336, 2013.

[5] Julien Marzat, Eric Walter, and Hélène Piet-Lahanier. Worst-case global optimization of black-box functions through kriging and relaxation. *Journal of Global Optimization*, 55(4):707–727, 2013.

[6] Daniel W Apley, Jun Liu, and Wei Chen. Understanding the effects of model uncertainty in robust design with computer experiments. *Journal of Mechanical Design*, 128(4):945–958, 2006.

[7] Samee Ur Rehman, Matthijs Langelaar, and Fred van Keulen. Efficient kriging-based robust optimization of unconstrained problems. *Journal of Computational Science*, 5(6):872–881, 2014.

[8] Simon Moritz Göhler, Tobias Eifler, and Thomas J Howard. Robustness metrics: Consolidating the multiple approaches to quantify robustness. *Journal of Mechanical Design*, 138(11):111407, 2016.

[9] Virginie Gabrel, Cécile Murat, and Aurélie Thiele. Recent advances in robust optimization: An overview. *European journal of operational research*, 235(3):471–483, 2014.

[10] Amadeu Almeida Coco, Elyn L Solano-Charris, Andréa Cynthia Santos, Christian Prins, and Thiago Ferreira de Noronha. Robust optimization criteria: state-of-the-art and new issues. *Technical Report UTT-LOSI-14001, ISSN: 2266-5064*, 2014.

[11] Renata Troian, Koji Shimoyama, Frédéric Gillot, and Sébastien Besset. Methodology for the design of the geometry of a cavity and its absorption coefficients as random design variables under vibroacoustic criteria. *Journal of Computational Acoustics*, 24(02):1650006, 2016.

[12] J. Darlington, C.C. Pantelides, B. Rustem, and B.A. Tanyi. An algorithm for constrained nonlinear optimization under uncertainty. *Automatica*, 35(2):217 – 228, 1999.

[13] Carl Edward Rasmussen and Christopher K. I. Williams. *Gaussian processes for machine learning*. Adaptive Computation and Machine Learning. MIT Press, Cambridge, MA, 2006.

[14] Loic Le Gratiet. *Multi-fidelity Gaussian process regression for computer experiments*. PhD thesis, Université Paris-Diderot-Paris VII, 2013.

[15] Tobias Wagner, Michael Emmerich, André Deutz, and Wolfgang Ponweiser. On expected-improvement criteria for model-based multi-objective optimization. In *International Conference on Parallel Problem Solving from Nature*, pages 718–727. Springer, 2010.

[16] Joshua Knowles. Parego: A hybrid algorithm with on-line landscape approximation for expensive multiobjective optimization problems. *IEEE Transactions on Evolutionary Computation*, 10(1):50–66, 2006.

[17] Wudong Liu, Qingfu Zhang, Edward Tsang, Cao Liu, and Botond Virginas. On the performance of metamodel assisted moea/d. In *International Symposium on Intelligence Computation and Applications*, pages 547–557. Springer, 2007.

[18] Qingfu Zhang, Wudong Liu, Edward Tsang, and Botond Virginas. Expensive multiobjective optimization by moea/d with gaussian process model. *IEEE Transactions on Evolutionary Computation*, 14(3):456–474, 2010.

[19] Wolfgang Ponweiser, Tobias Wagner, Dirk Biermann, and Markus Vincze. Multiobjective optimization on a limited budget of evaluations using model-assisted S-metric selection. In *International Conference on Parallel Problem Solving from Nature*, pages 784–794. Springer, 2008.

[20] Mickael Binois. *Uncertainty quantification on pareto fronts and high-dimensional strategies in bayesian optimization, with applications in multi-objective automotive design*. PhD thesis, Ecole Nationale Supérieure des Mines de Saint-Etienne, 2015.

[21] Michael TM Emmerich, André H Deutz, and Jan Willem Klinkenberg. Hypervolume-based expected improvement: Monotonicity properties and exact computation. In *Evolutionary Computation (CEC), 2011 IEEE Congress on*, pages 2147–2154. IEEE, 2011.

[22] Joshua Svenson and Thomas Santner. Multiobjective optimization of expensive-to-evaluate deterministic computer simulator models. *Computational Statistics & Data Analysis*, 94:250–264, 2016.

[23] Victor Picheny. Multiobjective optimization using gaussian process emulators via stepwise uncertainty reduction. *Statistics and Computing*, 25(6):1265–1280, 2015.

[24] Nadine Henkenjohann and Joachim Kunert. An efficient sequential optimization approach based on the multivariate expected improvement criterion. *Quality Engineering*, 19(4):267–280, 2007.

[25] Shinkyu Jeong and Shigeru Obayashi. Efficient global optimization (ego) for multi-objective problem and data mining. In *Evolutionary Computation, 2005. The 2005 IEEE Congress on*, volume 3, pages 2138–2145. IEEE, 2005.

[26] Luc Pronzato and Éric Thierry. Robust design with nonparametric models: prediction of second-order characteristics of process variability by kriging1. *IFAC Proceedings Volumes*, 36(16):537 – 542, 2003. 13th IFAC Symposium on System Identification (SYSID 2003), Rotterdam, The Netherlands, 27-29 August, 2003.

[27] Hans-Georg Beyer and Bernhard Sendhoff. Robust optimization – a comprehensive survey. *Computer Methods in Applied Mechanics and Engineering*, 196(33):3190 – 3218, 2007.

[28] Michael L. Stein. *Interpolation of spatial data*. Springer Series in Statistics. Springer-Verlag, New York, 1999. Some theory for Kriging.

[29] Delphine Dupuy, Céline Helbert, Jessica Franco, et al. Dicedesign and diceeval: Two r packages for design and analysis of computer experiments. *Journal of Statistical Software*, 65(11):1–38, 2015.

[30] David Ginsbourger, Rodolphe Le Riche, and Laurent Carraro. Kriging is well-suited to parallelize optimization. In *Computational Intelligence in Expensive Optimization Problems*, pages 131–162. Springer, 2010.

[31] John A Hartigan and Manchek A Wong. Algorithm as 136: A k-means clustering algorithm. *Journal of the Royal Statistical Society. Series C (Applied Statistics)*, 28(1):100–108, 1979.

[32] David Allen Van Veldhuizen. *Multiobjective Evolutionary Algorithms: Classifications, Analyses, and New Innovations*. PhD thesis, Wright Patterson AFB, OH, USA, 1999. AAI9928483.

[33] Jason R Schott. Fault tolerant design using single and multicriteria genetic algorithm optimization. Technical report, AIR FORCE INST OF TECH WRIGHT-PATTERSON AFB OH, 1995.

[34] Kalyanmoy Deb, Amrit Pratap, Sameer Agarwal, and TAMT Meyarivan. A fast and elitist multiobjective genetic algorithm: Nsga-ii. *IEEE transactions on evolutionary computation*, 6(2):182–197, 2002.

[35] E. Zitzler and L. Thiele. Multiobjective evolutionary algorithms: a comparative case study and the strength pareto approach. *IEEE Transactions on Evolutionary Computation*, 3(4):257–271, Nov 1999.

[36] Carlos A Coello Coello and Margarita Reyes Sierra. A study of the parallelization of a coevolutionary multi-objective evolutionary algorithm. In *Mexican International Conference on Artificial Intelligence*, pages 688–697. Springer, 2004.

[37] Carlos M. Fonseca, Luís Paquete, and Manuel López-Ibáñez. An improved dimension-sweep algorithm for the hypervolume indicator. In *Proceedings of the 2006 Congress on Evolutionary Computation (CEC 2006)*, pages 1157–1163. IEEE Press, Piscataway, NJ, July 2006.

Appendices

A Number of points for the estimation of the empirical variance

Let $\mathbf{x} \in D \subset \mathbb{R}^p$, an observation point. Let $\mathbf{H} \sim \mathcal{N}(0_{\mathbb{R}^p}, \Delta^2)$ be the random variable such as $\mathbf{x} + \mathbf{H} \sim \mathcal{N}(\mathbf{x}, \Delta^2)$ where Δ^2 is defined by:

$$\Delta^2 = \begin{pmatrix} \delta_1^2 & 0 & \dots & 0 \\ 0 & \delta_2^2 & \ddots & 0 \\ \vdots & \ddots & \ddots & \vdots \\ 0 & \dots & 0 & \delta_p^2 \end{pmatrix}$$

Let

$$\begin{array}{rccc} f: & \mathbb{R}^p & \longrightarrow & [a;b] \\ & \mathbf{x} & \longmapsto & f(\mathbf{x}) \end{array}$$

be a 2 times differentiable bounded function, where $a \in \mathbb{R}$ and $b \in \mathbb{R}$. Then all the moments of $f(\mathbf{x} + \mathbf{H})$ exist. Let introduce the moments $\mu = \mathbb{E}(f(\mathbf{x} + \mathbf{H}))$, $v_f = Var(f(\mathbf{x} + \mathbf{H}))$ and $\mu_4 = \mathbb{E}\left[(f(\mathbf{x} + \mathbf{H}) - \mu)^4\right]$. Let $\bar{F} = \frac{1}{n}\sum_{i=1}^n f(\mathbf{x} + \mathbf{H}^i)$ be the empirical estimator of μ where $\mathbf{H}^1, \dots, \mathbf{H}^n$ is an n sampling of the random variable $\mathbf{H}$ and $S^2 = \frac{1}{n}\sum_{i=1}^n (f(\mathbf{x} + \mathbf{H}^i) - \bar{F})^2$ the empirical estimator of v_f. Classical results on convergence of moments estimators imply that:

$$\sqrt{n}(S^2 - v_f) \longrightarrow^{\mathcal{L}} \mathcal{N}(0, \mu_4 - v_f^2)$$

As the emprical estimator $\hat{\mu}_4$ converges in probability to μ_4, asymptotically

$$\frac{S^2 - v_f}{\sqrt{(\hat{\mu}_4 - v_f^2)/n}} \sim \mathcal{N}(0, 1)$$

Let z the quantile of the standard normal distribution of a risk α, then:

$$\mathbb{P}\left(\left|\frac{S^2 - v_f}{\sqrt{(\hat{\mu} - v_f)^2/n}}\right| \leq z\right) = 1 - \alpha$$

To obtain a range on v_f with probability $1 - \alpha$, we have to solve the following inequality

$$\left|\frac{S^2 - v_f}{\sqrt{(\hat{\mu}_4 - v_f^2)/n}}\right| \leq z \Leftrightarrow \left(1 + \frac{z^2}{n}\right) v_f^2 - 2S^2 v_f + \left((S^2)^2 - \frac{z^2 \hat{\mu}_4}{n}\right) \leq 0.$$

The discriminant $\Delta = \frac{4z^2}{n}\left(\hat{\mu}_4\left(1 + \frac{z^2}{n}\right) - (S^2)^2\right)$, is positive if $\hat{\mu}_4\left(1 + \frac{z^2}{n}\right) > (S^2)^2$.
The Jensen Inequality (convexity) implies that :

$$\frac{1}{n}\sum_{i=1}^n (f(x + H^i) - \bar{F})^4 \geq \left(\frac{1}{n}\sum_{i=1}^n (f(x + H^i) - \bar{f})^2\right)^2 \Leftrightarrow \hat{\mu}_4 \geq (S^2)^2$$

Then $\Delta > 0$ and

$$v_f \in \left[\frac{2S^2 - \sqrt{\Delta}}{2\left(1 + \frac{z^2}{n}\right)}; \frac{2S^2 + \sqrt{\Delta}}{2\left(1 + \frac{z^2}{n}\right)}\right]$$

Using a Taylor approximation of order $o\left(\frac{1}{n}\right)$, we obtain that

$$v_f \in \left[S^2 - \frac{z}{\sqrt{n}}\sqrt{\hat{\mu}_4 - (S^2)^2}; S^2 + \frac{z}{\sqrt{n}}\sqrt{\hat{\mu}_4 - (S^2)^2}\right]$$

In order to obtain an approximation error lower or equal to ϵ, we choose:

$$n > \frac{z^2}{\epsilon^2}(\hat{\mu}_4 - (s^2)^2)$$

where s^2 (resp. $\hat{\mu}_4$) is a first estimation of the second (resp. the fourth) central moment.